Simulation on Helicopter Scissors Tail-Rotor Noise Based on N-S Equations and F1A Formulas

Meng Xiaowei, *Xu Guohua* *, *Shi Yongjie*, *Wang Liangquan*

National Key Laboratory of Rotorcraft Aeromechanics, Nanjing University of Aeronautics
and Astronautics, Nanjing 210016, P. R. China

(Received 4 November 2016; revised 24 April 2017; accepted 25 May 2017)

Abstract: Aiming at the noise of helicopter scissors tail-rotor, an advanced numerical method is established by combining computational fluid dynamics (CFD) model with Farassat 1A (F1A) formula. In this method, Navier-tokes (N-S) equations are used as governing equations, and the flow field is solved at quasi-steady and unsteady states in hover and forward fight, respectively, based on two different types of embedded grid systems. A simple and effective solution approach is provided for the generation difficulty of donor cells caused by the close gap among scissors tail-rotor blades. Using the CFD calculation results as input, the thickness noise, loading noise and total noise of tail-rotor are calculated by F1A formula. By the method, numerical examples on rotor flowfield and noise are performed and the results are compared with available data. Then, aerodynamic and acoustic characteristics of scissors tail-rotor are emphatically calculated in both hover and forward flight. Furthermore, the research on the effects of blade-tip shape parameters on scissors tail-rotor noise is carried out. Also, the scissors tail-rotor is compared with the conventional tail-rotor, and the results show that in hover, the noise of a scissors tail-rotor is not always the smaller one.

Key words: FW-H equation; scissors tail rotor; thickness noise; loading noise; helicopter; computational fluid dynamics (CFD)

CLC number: V211.52 **Document code**: A **Article ID**: 1005-1120(2017)06-0710-10

0 Introduction

The acoustic signature radiated by helicopter is an important concern in both civil and military operations. In addition to the rotor noise, the tail-rotor is a prime external noise source, and the aerodynamic noise of tail-rotor contributes to the overall noise level of a helicopter. In some flight regimes, the noise of the tail-rotor is even greater than that of the main rotor[1]. Therefore, the study on noise characteristics of helicopter tail-rotor is of great significance.

Currently, helicopter tail-rotors mainly have three types, including conventional tail-rotor (CTR), scissors tail-rotor (STR) and ducted tail-rotor (DTR). As a ″new″ type, STR has been applied to modern armed helicopters, such as ″Apache″ in USA and ″Holocaust in Russia. The difference between STR and CTR is that the former has uneven distribution of blades and there is an axial spacing between its upside and downside pairs of blades. Previous research has suggested that STR might possess a certain noise reduction potential, compaired to CTR[2]. On the other hand, because of the unique configuration of STR, especially the narrow axial spacing between the upside and downside blades, blade vortex interaction (BVI) may be severer in some flight regime. Therefore, compared with CTR, aerodynamic and noise characteristics for STR are more complex. So far, a lot of research work on the aerodynamic noise of a helicopter rotor or a CTR

---

* Corresponding author, E-mail address: ghxu@nuaa.edu.cn.

How to cite this article: Meng Xiaowei, Xu Guohua, Shi Yongjie, et al. Simulation on helicopter scissors tail-rotor noise based on N-S equations and F1A formulas[J]. Trans. Nanjing Univ. Aero. Astro., 2017,34(6):710-719.
http://dx.doi.org/10.16356/j.1005-1120.2017.06.710

has been conducted, but the studies on STR′s noise are few at home and abroad. In Ref. [2], the experimental test for STR in hover was performed in 1996, and the noise level of M-28 helicopter with CTR was compared with that of M-28 helicopter with STR. The measured results indicated that the noise of STR was lower than that of CTR. Ref. [3] investigated the effect of uneven angle among blades on rotor noise, but its experimental model was not for the STR, only for main rotor, and it excluded the axial spacing of actual scissors configuration. At home, some preliminary studies for STR′s aerodynamic and noise characteristics were carried out previously through test and computational analysis[4-6] for the hovering state, but detailed parametric analysis for the STR′s noise was not performed.

Therefore, an advanced numerical method combining the CFD technology with F1A formula is established to investigate the STR′s aerodynamic and noise characteristics in this paper. The method is firstly used to calculate aerodynamic loadings on the blade surface of the tail-rotor by CFD modules, and secondly to calculate the aerodynamic noise. For the convenience of the flow field solution on STR, a structured embedded grid system is generated. However, because of the scissors angle of STR, the separation between two blade roots is very close and thus, when generating blade grid, the outermost grid layer of a blade will easily collide with another blade′s surface, which will increase the difficulties of digging holes. To this end, we present a simple and effective solution. To analyze the STR′s noise better, a so-called hemisphere is introduced to observe the noise of STR, and some observation points are located on the surface of the hemisphere.

Many studies on the influence of helicopter rotor blade-tip shape parameters on noise have been conducted, but seldom for the STR. Therefore, the investigation on the influence of the STR blade-tip shape parameters is also carried out in this paper, and the variation trend of the noise for different parameters is calculated and analyzed. Some meaningful conclusions are drawn.

Previous studies on noise of STR at hover condition in Refs. [2,6] concluded that the total noise of STR was smaller than that of CTR along the main radiation direction[7] of total noise. However, studies in this paper indicate that their conclusion is obtained based on the condition at which severe BVI between the vortex shed from the upside blades and the downside blades does not occur.

1 Methodology Description

1.1 CFD method

The unsteady Reynolds averaged Navier-Stokes (N-S) equations are utilized as the governing equations, and the expression[8] is presented as

$$\frac{\partial}{\partial t}\iiint_V \boldsymbol{W}\mathrm{d}V + \oiint \boldsymbol{F}\cdot\boldsymbol{n}\mathrm{d}S - \oiint \boldsymbol{G}\cdot\boldsymbol{n}\mathrm{d}S = 0 \quad (1)$$

where S is the area, V the volume and $\boldsymbol{n}$ the outside vector of the cell surface. The conserved variable $\boldsymbol{W}$, the convective flux $\boldsymbol{F}$ and the viscous flux $\boldsymbol{G}$ are given by

$$\boldsymbol{W} = [\rho, \rho u, \rho v, \rho w, \rho E]^{\mathrm{T}} \quad (2)$$

$$\boldsymbol{F} = \begin{bmatrix} \rho(\boldsymbol{V}-\boldsymbol{V}_t) \\ \rho u(\boldsymbol{V}-\boldsymbol{V}_t) + p\boldsymbol{I}_x \\ \rho v(\boldsymbol{V}-\boldsymbol{V}_t) + p\boldsymbol{I}_y \\ \rho w(\boldsymbol{V}-\boldsymbol{V}_t) + p\boldsymbol{I}_z \\ \rho E(\boldsymbol{V}-\boldsymbol{V}_t) + p\boldsymbol{V} \end{bmatrix} \quad (3)$$

$$\boldsymbol{G} = \begin{bmatrix} 0 \\ \tau_{xx}\boldsymbol{I}_x + \tau_{xy}\boldsymbol{I}_y + \tau_{xz}\boldsymbol{I}_z \\ \tau_{xy}\boldsymbol{I}_x + \tau_{yy}\boldsymbol{I}_y + \tau_{yz}\boldsymbol{I}_z \\ \tau_{xz}\boldsymbol{I}_x + \tau_{yz}\boldsymbol{I}_y + \tau_{zz}\boldsymbol{I}_z \\ g_x\boldsymbol{I}_x + g_y\boldsymbol{I}_y + g_z\boldsymbol{I}_z \end{bmatrix} \quad (4)$$

where $\boldsymbol{V} = [u, v, w]^{\mathrm{T}}$ is the absolute velocity and $\boldsymbol{V}_t$ the normal velocity of cell boundary.

The cell-centered finite volume method is adopted for spatial discretization. The Roe scheme[9] is selected as the dimensional discrete format to discretize the governing equations.

For time discretization, the efficient and implicit lower-upper symmetric Gauss-Seidel (LU-SGS) scheme[10] is applied to the pseudo-time step of the dual time method. This method is carried out in two steps

(1) Forward sweep

$$\Delta \boldsymbol{W}_j^* = D^{-1}\Big[-R_i - \sum_{j:j<i}\frac{1}{2}\big(\Delta F(\boldsymbol{W}_j^*, \boldsymbol{n}_{ij}) - |\lambda_{ij}|\Delta \boldsymbol{W}_j^*\big)|S_{ij}|\Big] \tag{5}$$

(2) Backward sweep

$$\Delta \boldsymbol{W}_j^* = \Delta \boldsymbol{W}_j^* - D^{-1}\sum_{j:j>i}\frac{1}{2}\big(\Delta F(\boldsymbol{W}_j^*, \boldsymbol{n}_{ij}) - |\lambda_{ij}|\Delta \boldsymbol{W}_j^*\big)|S_{ij}| \tag{6}$$

where $|\lambda_{ij}|$ is the spectral radius of flux Jacobian matrices, $|S_{ij}|$ the area of interface and drepresents the diagonal matrix.

In addition, the Spalart-Allmaras one-equation model[11] is used as the turbulence model.

1.2 Embedded grid technology

The embedded grid technology[12] is utilized including blade grids and a background grid covering the whole calculation domain. There are two technical difficulties on the embedded grids generation, i. e., holes digging and donor cells searching. Here, the Hole Map scheme[13] is used for digging holes, and the strategy proposed in Ref. [14] is adopted to search donor cells. The background grid used in this study has 2 overlaid levels, Level 1 (fine) and Level 2 (coarse). Fig. 1 (a) illustrates this multi-level grid concept. Structured grid is employed for background grids and C-O type grid is adopted for blade grids. In order to better capture the aerodynamic characteristics on blade surface, the tail-rotor disk domain in background grid is overlaid by fine grid, which is also beneficial to search the donor cells. It should be noticed that the gap between two blade roots becomes smaller because of the scissors angle of STR, and when generating the blade grids, the outermost layer of the blade grids is not allowed to encounter the surface of another blade to ensure holes digging smoothly, so the separation between the outermost layer of blade grids and blade surface should be limited. On the other hand, if the gap is too small, the calculation accuracy of loadings will be influenced. The main contribution of the blade loadings comes from the tip segment of blade. Therefore, thinning the blade-root grids and thickening the blade-tip grids is a reasonable choice. The specific process is as follows: (1) Two-dimensional airfoil grids are generated for blade root section and blade tip section, respectively, and the separation from outermost layer of grids to the airfoil surface should be properly controlled to make the scope of two-dimensional grids of blade root section smaller than that of the blade tip section; (2) when generating 3-D blade grids, blade grids becomes thicker gradually from blade root to blade tip by linear interpolation. Note that the number of layers for blade-root section and blade-tip section grids should be set equal to avoid mistakes while generating the blade grids. The schematics of blade grids and 2-D sectional airfoil grids are shown in Fig1 (b).

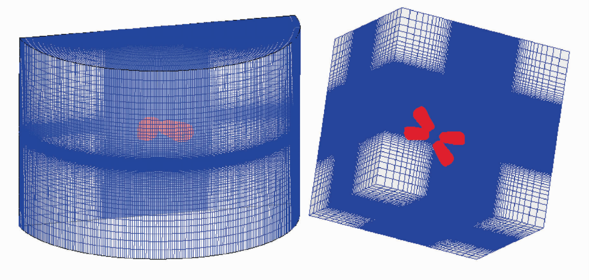

(a) Girds in hover(left) and forward flight(right)

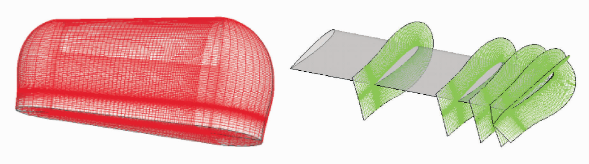

(b) Blade and section grids

Fig. 1 Schematic of embedded grid system

1.3 Acoustic model

The sound pressure of thickness noise is calculated using Eq. (7) and the sound pressure of loading noise is calculated by Eq. (8). The sound pressure of total noise can be obtained using Eq. (9) (F1A formula)[15]

$$4\pi p'_T(\boldsymbol{x}, t) = \int_{f=0}\left[\frac{\rho_0(\dot{v}_n + v_{\dot{n}})}{r(1-M_r)^2}\right]_{\mathrm{ret}}\mathrm{d}S +$$

$$\int_{f=0}\left[\frac{\rho_0 v_n(r\dot{M}_r + a_0(M_r - M^2))}{r^2(1-M_r)^3}\right]_{\mathrm{ret}}\mathrm{d}S \tag{7}$$

$$\begin{aligned}4\pi p'_L(\boldsymbol{x},t) = &\int_{f=0}\left[\frac{\dot{l}_r}{r(1-M_r)^2}\right]_{\mathrm{ret}}\mathrm{d}S + \\ &\int_{f=0}\left[\frac{l_r - l_M}{r^2(1-M_r)^2}\right]_{\mathrm{ret}}\mathrm{d}S + \\ &\frac{1}{a_0}\int_{f=0}\left[\frac{l_r(r\dot{M}_r + a_0(M_r - M^2))}{r^2(1-M_r)^3}\right]_{\mathrm{ret}}\mathrm{d}S\end{aligned} \tag{8}$$

$$p'(\boldsymbol{x},t) = p'_T(\boldsymbol{x},t) + p'_L(\boldsymbol{x},t) \tag{9}$$

where p' is the disturbed sound pressure, a_0 the speed of sound, ρ_0 the density, v_n the normal velocity on blade surface, l_i the force per unit area on the fluid, $l_i = P_{ij}\hat{\boldsymbol{n}}_j$, P_{ij} the compressive stress tensor that includes the surface pressure and viscous stress, $\hat{\boldsymbol{n}}_j$ the unit outward normal vector on the blade surface, r the distance from the source surface to the observation point, and Ma_r the Mach number in the radiation direction. l_r the force on the fluid per unit area in the radiation direction, $l_r = l_i\hat{\boldsymbol{r}}_i$, $\hat{\boldsymbol{r}}_i$ the unit radiation vector. The dots on $\dot{v}_n$, $\dot{M}_r$ and $\dot{l}_r$ denote the rate of variation with respect to source time. p'_T, p'_L and p' denote sound pressure of thickness noise, loading noise and total noise, respectively.

1.4 Validation of calculation methods

The tail-rotor's test data is rare, so similar main rotor was chosen for validation. CFD validations include Caradonna-Tung rotor hover test[16] and Helishape 7A rotor forward-flight test[17]. The 1/7 UH-1H rotor model[18] was taken as the noise calculation example. As shown in Figs. 2—4, the calculation results match well with the data of previous studies, which demonstrates the capability of the present method in calculating the tail-rotor's aerodynamic and noise characteristics.

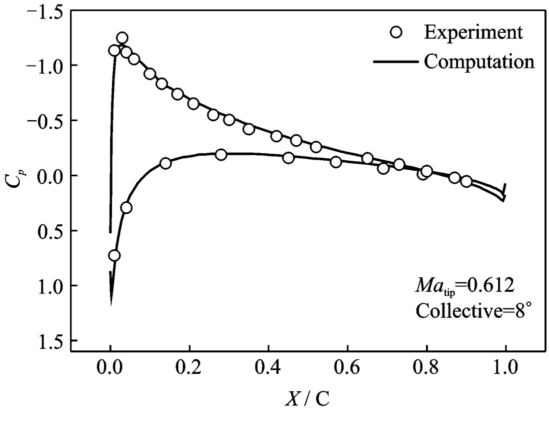

Fig. 2 Comparisons of calculated C_p with data at 0.89R section for C-T rotor in hover

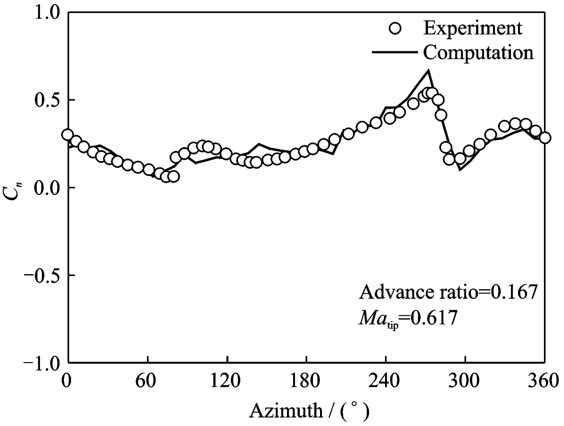

Fig. 3 Comparisons of calculated C_n with data for Helishape 7A rotor in forward flight

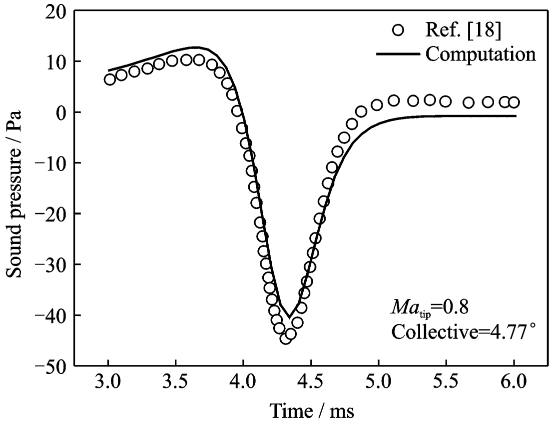

Fig. 4 Comparisons of calculated sound pressure with Baeder's result for UH-1H rotor

2 Aerodynamic and Acoustic Analysis of STR

The Mi-28 tail-rotor[2] was chosen as baseline case, and the configuration parameters were changed so as to be more suitable for the present study. The specific parameters are shown in Table 1. The test of STR configuration in Ref. [4] has shown that the aerodynamic characteristics of configuration L are better than that of configuration U, so configuration L shown in Fig. 5 is adopted. If the scissors angle is 90° and the axial spacing is 0, STR will be simplified to CTR.

Table 1 Parameters of STR

No.	Radius/m	Chord/m	Airfoil	Twist/(°)	Configuration
4	1.35	0.22	NACA0012	0	L

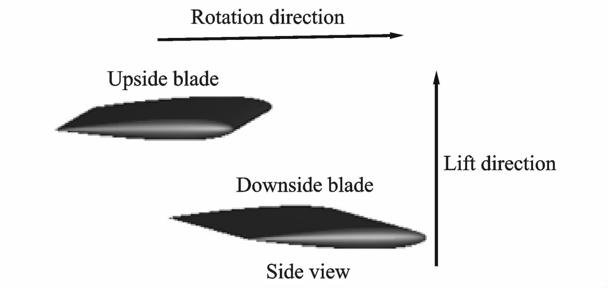

Fig. 5 The schematic of configuration L

2.1 Aerodynamics comparison between STR and CTR

The comparisons of aerodynamic characteristics between STR and CTR in hover and forward flight are analyzed in this section. Figs. 6(a, b) present the overall vorticity contours of CTR and STR in hover (vorticity is equal to 0.31). As shown in Fig. 6, the vortex wake of STR is different from that of CTR in hover obviously, and the former is more disorganized. Since the tip vortexes of the upside blades collide directly with the downside blades, obvious BVI occurs on STR, which impacts blade aerodynamic characteristics and loading noise.

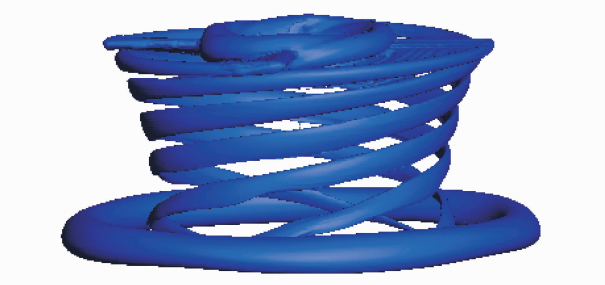

(a) CTR

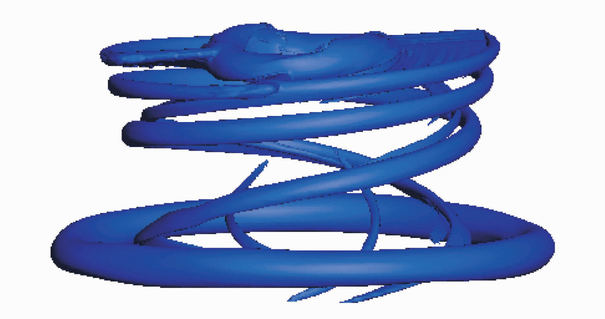

(b) STR

Fig. 6 Vorticity comparison of STR and CTR

Fig. 7 illustrates the normal force coefficient versus azimuthal angle at $r=0.91R$. The calculated parameters are as follows: Advanced ratio of 0.2, blade tip Mach number of 0.62 and collective angle of 8°. As seen in Fig. 7, the loadings at the azimuth of 100° and 280° are bigger and change more quickly for CTR. However, the normal force peaks of downside blade section for STR appear earlier (93° and 267°) due to the scissors angle. Also, the normal forces of upside blade change more gently than that of downside blade for STR, apparently because the interaction of downside blade on upside blade is weaker. The loading variation will directly affect the noise, which can be learned in next section.

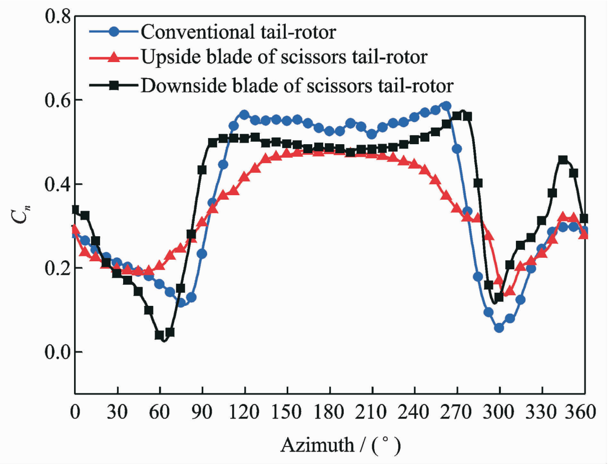

Fig. 7 Normal force coefficient along different azimuthal angles ($r=0.91R$, $u=0.2$)

2.2 Noise comparison of STR and CTR

As shown in Fig. 8, a hemisphere is used for noise observation. For convenience, the tail rotor disk is placed in horizontal plane, and the direction and amplitude of noise are analyzed in hover and forward flight.

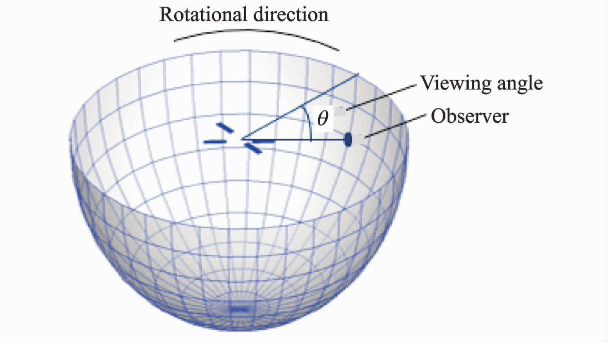

Fig. 8 Hemisphere surface

Fig. 9 presents the noise sound pressure level (SPL) contours of STR and CTR at the hover condition in which the blade-tip Mach number is 0.62 and the collective is 10°. For convenience, the three-dimensional hemispherical surface is transformed into a two-dimensional plane by Lambert projection method. As seen from Fig. 9, for both CTR and STR configurations, the main radiation direction of the total noise is along the disk plane. The SPL of total noise decreases rapidly with the increase of observation angle and the noise difference between 45° observation angle and disk-plane reaches more than 6 dB. Moreover, the main radiation direction of thickness noise is along disk plane while the loading noise is not, which was also obtained in the calculation (not shown). In addition, the main radiation direction of the total noise is consistent with that of thickness noise, so thickness noise is dominated at the condition.

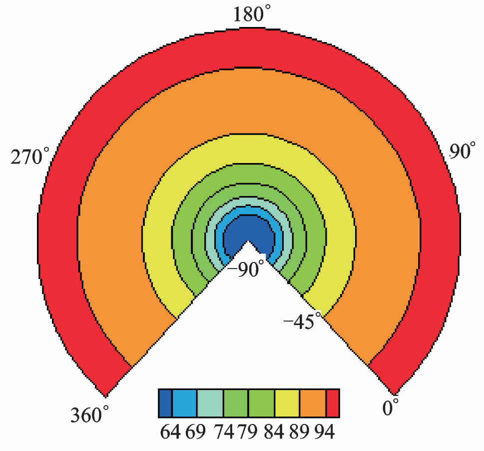

(a) CTR

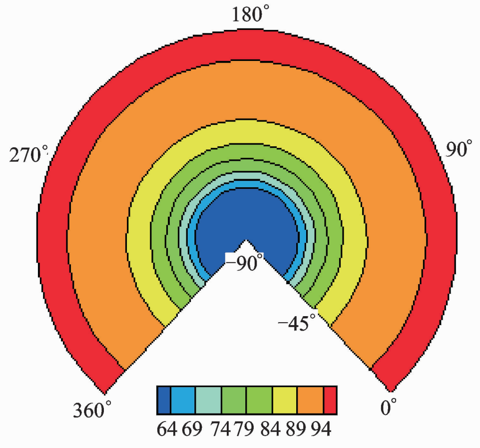

(b) STR

Fig. 9 Total noise SPL contours of CTR and STR

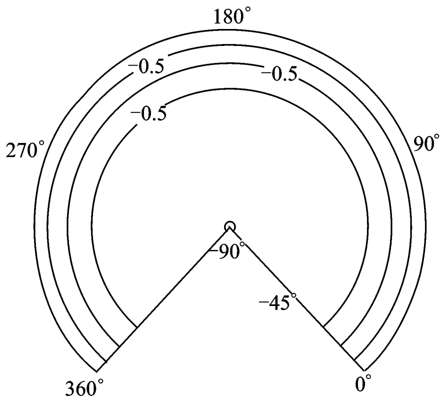

(a) Difference of thickness noise

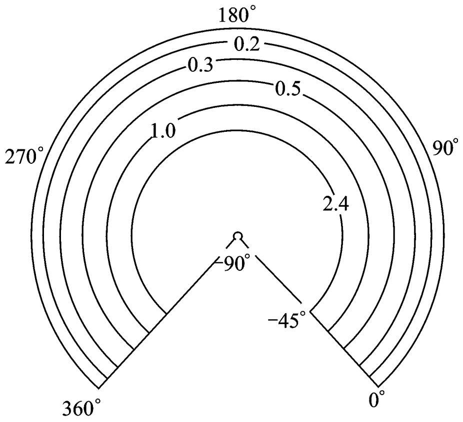

(b) Difference of total noise

Fig. 10 Noise difference between STR and CTR

Previous research has shown that STR may reduce the noise of the tail-rotor to some extent because of its "modulation effect"[6]. In the above section, it is shown that the collision of upside blade′s tip vortex with downside blade may increase the loading and total noises. Fig. 10 demonstrates the difference of total noise (STR′s noise values minus CTR′s) at this condition. As shown in Fig. 10 (a), the thickness noise SPL of STR is less than CTR′s (difference is negative) in the disk plane direction (main radiation direction of thickness noise), which indicates that STR is of the noise reduction potential when thickness noise is dominant. Here, it should be noted that the difference will change with different observation angles. Since the main radiation direction of thickness noise is along disk plane at this condition, only the difference near the disk plane is shown. The difference changes slightly near disk plane, so the values of three isolines are same after keeping one decimal place. However, from

Fig. 10 (b), the total noise of STR is slightly larger than that of CTR′ instead in the main radiation direction (difference is positive), because the thickness noise′s dominance is weakened with the increase of loading noise at the condition with serious BVI on STR. Further, due to the BVI between upside and downside blades, the STR′s loading noise is greater than CTR′s, but the CTR does not have such strong BVI because its four blades are on the same plane. Fig. 10 also shows that the difference is getting bigger with the increase of observation angle. Comparing Fig. 10 (a) with Fig. 10 (b), a conclusion is drawn as follows: At the condition of serious BVI, although thickness noise of STR is still less than CTR′s, loading noise of STR is larger, thereby STR′s total noise can be slightly larger than the CTR′s.

Fig. 11 shows the comparison of total noise sound pressure history between STR and CTR at the observation angle of 40°. Obviously, the former sound pressure peak changes more sharply than the latter, which is consistent with the result that the total noise SPL of STR is about 2.2 dB higher than the CTR′s in Fig. 10(b). Besides, the azimuths at which their peak noises appear are different due to the presence of the scissors angle.

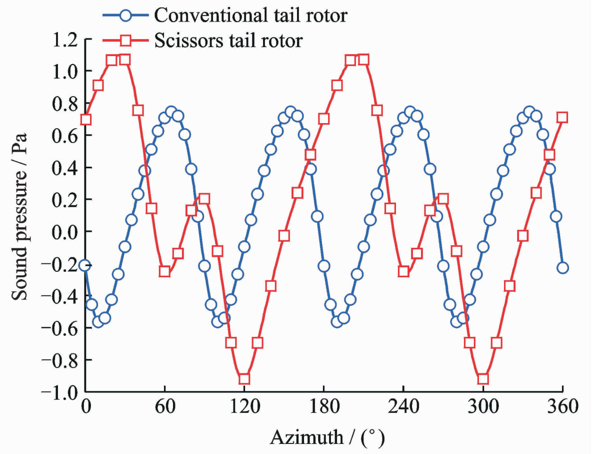

Fig. 11 Comparison of total noise sound pressure history between STR and CTR at the observation angle of 40°

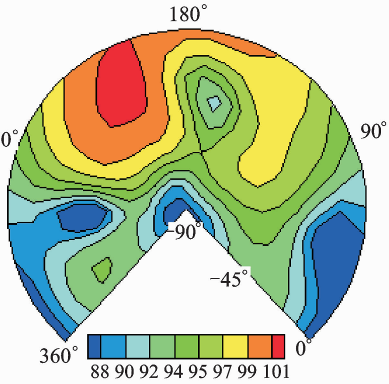

(a) CTR

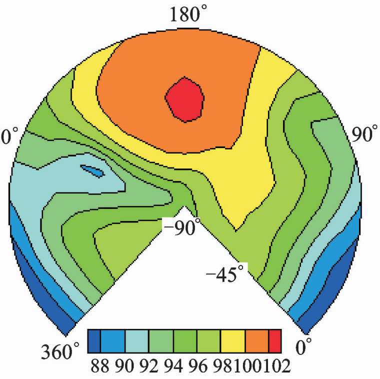

(b) STR

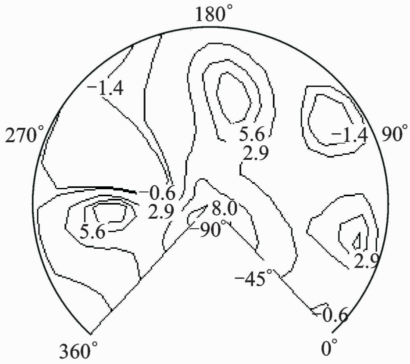

(c) The noise difference

Fig. 12 Total noise SPL contours and noise difference map of STR and CTR

Fig. 12 presents the noise SPL contours and the difference between STR and CTR at an advanced ratio of 0.2, a blade-tip Mach number of 0.62 and a collective of 8°. As seen in Figs. 12(a, b), compared with hover, the main radiation direction of total noise in forward flight moves forward (the azimuth of 180° in Fig. 12), and the value of noise in front of the disk is significantly greater than that in the rear. Compared with the hovering state, the main radiation direction of the total noise will no longer be along disk plane direction in forward flight, and shifts downward instead, because the loading noise is dominant at this condition, so the main radiation direction of the total noise is almost consistent with that of the loading noise. Comparing the main radiation direction of STR′s noise with CTR′s one, it is known that the former is mainly along the front and below, however, the later shifts toward the retreating side. Comparing their noise amplitude, it can be seen (Fig. 12(c)) that the total noise of STR is much bigger than that of CTR forward and below (about 5.6 dB), but in the main radiation direction of the total noise of CTR, the total noise of STR is about 1 dB smaller than that of CTR.

The reason why the main radiation direction of their total noise is inconsistent is as follows:

It can be seen from Eq. (4) that the parameters affecting the loading noise include l_r, $\dot{l}_r$ and M_r. From the analysis in Section 2.1, the azimuth angles at which the maximum variation gradient of blade loading (l_r) appears are different for STR and CTR, which will cause a distinction between the main radiation directions of the two configurations. Fig. 13 demonstrates their noise radiation directions. In Fig. 13, the solid lines represent STR while the dotted ones represent CTR. It is observed that when azimuth angle is 93°(see Fig. 7) for STR, M_r is the greatest in the front. Once M_r is greater, the loading noise will be greater in that direction, so the total noise of STR is almost the greatest both in the front of disk and below it. However, at azimuth angle of 100°(see Fig. 7) for CTR, the direction of $M_{r\max}$ for CTR moves toward the retreating side, and then the main radiation direction of total noise also moves toward the retreating side.

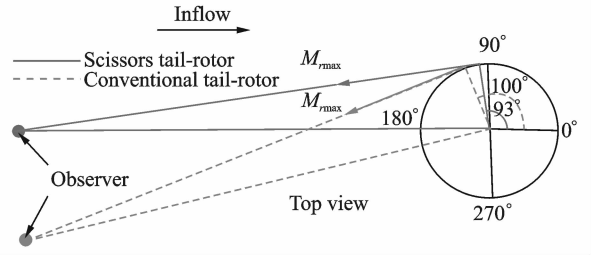

Fig. 13 The noise radiation direction

3 Influence of Blade-Tip Shape Parameters on STR Noise

For thickness noise, its amplitude is related to the movement rate and the geometry size of blades. In order to further examine the contribution of blade segment to thickness noise, Figs. 14 (a, b) show the different blade-tip segments and their thickness noise SPL proportion, respectively. The proportion is defined as the ratio of SPL contribution of corresponding segments to SPL of the whole blade. It is shown from Fig. 14 that with the increase of the tip segment length, the thickness noise proportion is also increasing, but the increase rate is very slow. It can also be seen from Fig. 14 that the thickness noise contribution of the segments (0.9R—1.0R) accounts for 92.8% of the whole thickness noise of blade. This means that tip segment is the main contributor of thickness noise (note: in Section 1.2, it is known that thickness noise is dominated at the condition). Therefore, the noises are analyzed by changing blade tip shapes later.

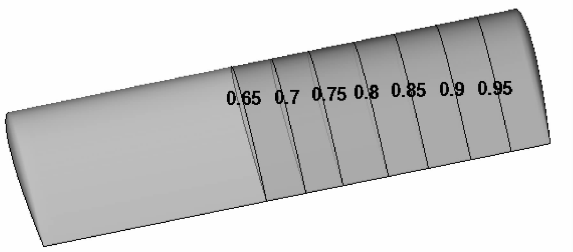

(a) Blade-tip segments

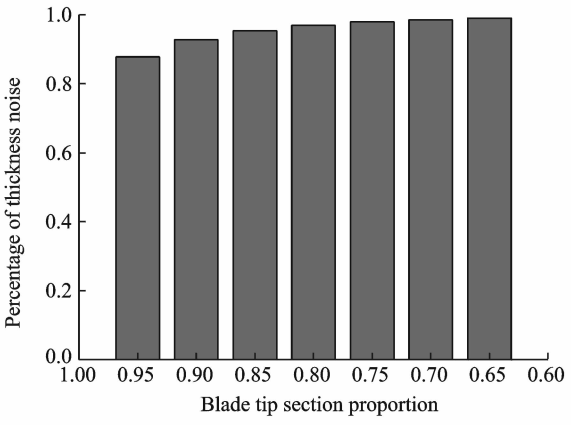

(b) Proportion of thickness noise

Fig. 14 Proportion of thickness noise with different segments

3.1 Influence of tip taper

Fig. 15 shows the noise SPL of STR with different tapered ratio from 0.9R. When the tapered ratio is 0.55, the thickness noise is 2.15 dB smaller when compared with rectangular tip, and the total noise reduces by 1.90 dB. It is seen from Fig. 15 that the noise decreases with reduction of tapered ratio, because the taper reduces the volume of the tail-rotor blades and accordingly decreases the thickness noise, so the total noise of the tail rotor is also reduced.

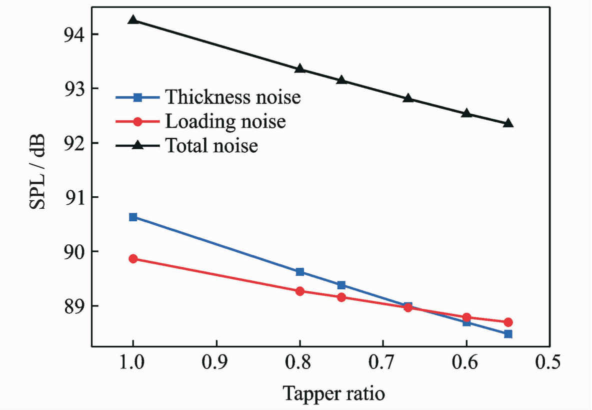

Fig. 15 SPL variation of noise with taper ratio

3.2 Influence of tip thickness

Table 2 shows the influence of tip thickness on total noise. As seen from the table, when the blade tip thickness reduces from 12% to 9% chord, the total noise can be slightly reduced.

Table 2 Influence of tip thickness on total noise

Blade tip segment	0.9—1R	0.85—1R
Variation in thickness/ (% chord)	12—9	12—9
Variation in noise/dB	−0.89	−1.09

The influence of sweep-back and anhedral blade tips on noise is also calculated, and the results indicate that their influence is very small and not shown here.

4 Conclusions

(1) In hover, compared with the noise of CTR, the noise of STR is not always smaller in all cases. When BVI is serious, the former's loading noise is greater than the latter's, and thus the total noise of the former can be greater than the latter's.

(2) In hover, the vortex wake of STR is obviously different from that of CTR. The former is more disorganized. This is because the tip vortex of the upside blade collide directly with the downside blade.

(3) In forward flight, due to the existence of scissors angle, the normal force peaks of downside blade section for STR appear earlier than that of CTR, while the normal force of the upside blade section changes relatively gently, because the interaction of downside blade on upside blade is weaker.

(4) Compared with the hover state, the main radiation direction of noise is along the front and below in forward flight, and the noise in front of the disk is significantly greater than that in the rear.

(5) In hover, compared with the inner parts of blade, the tip portion of STR contributes almost all of the thickness noise. If the blade tip is tapered and thinned, the SPL of the total noise will be reduced accordingly.

References:

[1] GREENWOOD E, SCHMITZ F H. Separation of main and tail rotor noise from ground-based acoustic measurements[J]. Journal of Aircraft, 2014,51(2): 464-472.

[2] ROZHDESTENSKY M G. Scissors rotor concept: New results obtained[C]//American Helicopter Society 52nd Annual Forum, D. C. Washington: [s. n.], 1996.

[3] EDWARDS B D. Psychoacoustic testing of modulated blade spacing for main rotor[R]. NASA CR-2002-211651, 2002.

[4] XU G H, WANG S C, ZHAO J G. Experimental and analytical investigation on aerodynamic characteristics of helicopter scissors tail rotor[J]. Chinese Journal of Aeronautics, 2001,14(4):193-199.

[5] XU G H, ZHAO Q J, PENG Y H. Study on the induced velocity and noise characteristics of a scissors rotor[J]. Journal of Aircraft, 2007,44(3):806-811.

[6] FAN F, SHI Y J, XU G H. Aerodynamics and noise characteristics of scissors tail rotor in hover[J]. Acta Aeronautica et Astronautica Sinica, 2013, 34(9): 2100-2109. (in Chinese)

[7] JOHNSON W. Helicopter theory[M]. Princeton University Press, 1980.

[8] BLAZEK J. Computational fluid dynamics: Principle and applications[M]. 2nd Ed. Elsevier Science Ltd, 2005.

[9] ROE P L. Approximate Riemann solvers, parameter vectors, and difference schemes[J]. Journal of Computational Physics, 1981,43(2):357-372.

[10] LUO H, BAUM J D. A fast, matrix-free implicit method for computing low Mach number flows on unstructured grids[R]. AIAA 99-3315, 1999.

[11] SPALART P R, ALLMARAS S R. A one-equation turbulence model for aerodynamic flows[R]. AIAA 92-0439, 1992.

[12] STRAWN R C, CARADONNA F X, DUQUE E P N. 30 years of rotorcraft computational fluid dynamics research and development[J]. Journal of the American Helicopter Society, 2006,51(1):5-21.

[13] CHIU I T, MEAKIN R L. On automating domain connectivity for overset grids[R]. AIAA 95-0854, 1995.

[14] LOHNER R, SHAROV D, LUO H, et al. Overlapping unstructured grid[R]. AIAA 01-0439, 2001.

[15] BRENTNER K S. Prediction of helicopter rotor discrete frequency noise[R]. NASA TM-87721, 1986.

[16] CARADONNA F X, TUNG C. Experimental and analytical studies of a model helicopter rotor in hover [R]. NASA TM-81232, 1981.

[17] BIAVA M, BINDOLINO G, VIGEVANO L. Single blade computations of helicopter rotors in forward flight[R]. AIAA 2003-52, 2003.

[18] BAEDER J D, GALLMAN J M, YU Y H. A computational study of the aeroacoustics of rotors in hover[R]. AIAA 93-4450, 1993.

Mr. **Meng Xiaowei** received his master degree in Nanjing University of Aeronautics and Astronautics in 2016. His research interests are helicopter tail rotor noise reduction.

Prof. **Xu Guohua** is currently a professor at Nanjing University of Aeronautics and Astronautics. His major research interests are helicopter free wake simulation and rotor computational fluid dynamics.

Dr. **Shi Yongjie** is currently an associate professor at Nanjing University of Aeronautics and Astronautics. His major research interests are helicopter aerodynamics and aeroacoustics.

Mr. **Wang Liangquan** is currently a Ph. D. candidate at Nanjing University of Aeronautics and Astronautics. His major research interests include helicopter aerodynamics and rotor noise active control.

(Executive Editor: Zhang Bei)